Astron. Astrophys. 344, 675–680 (1999)

ASTRONOMY AND ASTROPHYSICS

The strengths of termination shocks in magnetized mass-loaded flows

R.J.R. Williams, J.E. Dyson, and T.W. Hartquist

Department of Physics and Astronomy, The University, Leeds, England LS2 9JT, UK

Received 5 October 1998 / Accepted 11 December 1998

Abstract. We adopt the Weber & Davis (1967) description of the dynamics of a magnetized isothermal outflow and add a constant source term to the continuity equation within a specified radius. Steady solutions to the outflow problem are calculated for various choices of free parameters. The fast-mode Mach numbers of fast-mode shocks in the mass-loading regions are calculated on the assumption that jump conditions must connect the preshock flow to the solution which passes smoothly through the fast-mode speed at the edge of the mass-loading region. Where the mass loading stagnates the flow, the fast-mode shock Mach numbers are often little greater than unity. The mass loading can result in the energy transport rate at the shock being reduced significantly from that in the gas at small radii. The results are of relevance to other divergent, magnetized, mass-loaded flows including those at boundary layers.

Key words: MHD – shock waves – ISM: magnetic fields

1. Introduction

In the construction of hydrodynamic models of time-dependent, spherically symmetric, mass-loaded, isothermal winds in planetary nebulae, Arthur et al. (1994) found that in evolved systems the termination shock often occurs at a Mach number much lower than that of the wind near the source. To explore the strengths of termination shocks in evolved mass-loaded isothermal winds more fully, Williams et al. (1995) used a steady hydrodynamic model and confirmed more generally that in many evolved mass-loaded systems much of the wind energy will be dissipated in the mass-loading region rather than in the termination shock. If the mass-loading is continuous, the dissipation is smoothly distributed. Even if the mass loading results from the presence of discrete centres, only a fraction of the dissipation will occur in the strong bowshocks at their heads. Williams et al. (1995) suggested that their results are of relevance to the issue of radio quietness or loudness, as it is reasonable to speculate that the total energy injected into cosmic-ray electrons in a bubble is a monotonically increasing function of the energy dissipated in large-scale termination shocks.

The issue of distributed dissipation versus dissipation localized to shocks is also relevant to the problem of the maximum speed to which species, such as H_2, can be accelerated without dissociating or ionizing them. Malone et al. (1994), Dyson et al. (1995) and Raga et al. (1998) have proposed that gradual mass-loading in boundary layers can result in H_2 being accelerated to high speeds without passing through very strong shocks. The results of Williams et al. (1995) are of relevance to this issue as the boundary layer flows are divergent as well as mass-loaded, and the results for spherically symmetric flows show general properties that should characterise flows diverging in other geometries.

Diffuse astrophysical media are magnetized, and magneto-hydrodynamic (MHD) models rather than hydrodynamic models can be more appropriate. Thus, in this paper we report on a study of MHD models of steady, divergent, mass-loaded, isothermal winds. As a magnetic field is assumed to be present, the wind cannot, in reality, be spherically symmetric. We adopt a treatment of a magnetized wind due to Weber & Davis (1967) and add a continuous, distributed mass input to the flow. The equations used are presented in Sect. 2. While a mass source term is included in the equation of continuity, we assumed that the picked up material brings no magnetic field with it. While the clumps embedded in an astrophysical wind are magnetized, implying that this assumption may be invalid in many cases, it is less likely that the magnetic field advected into the flow from many loading centres will have a net overall orientation. The issue of the validity of the assumption will require a thorough understanding of intermediate-scale (i.e. the scale ranging from roughly the size of the clumps to the interclump spacing) and smaller scale behaviour, which does not exist at this time. Possibly the assumption is of some relevance in diverging flows for those boundary layers in which material on at least one side is only weakly ionized, allowing ambipolar diffusion of neutrals across field lines as they are picked up. Sect. 3 contains results including curves showing the radial velocity as a function of radius for each of a number of solutions and a table giving the fast-mode Mach number of the fast-mode shock that forms in the flow as a function of the maximum fast-mode Mach number that the flow attains for those solutions. We also give curves showing how the energy transport in the flow is divided between thermal, kinetic and electromagnetic components.

2. The equations

We consider a steady magnetized flow passing through a mass-loading zone. We assume that the mass-loading is spherically

Send offprint requests to: R.J.R. Williams (rjrw@ast.leeds.ac.uk)

stratified, and ignore all derivatives in θ and ϕ. It is apparent that mass-loading centres give rise to strong radial magnetic fields in their tails (e.g. Dgani & Soker 1998) as the azimuthal field incident head-on is impeded by the bowshock, as in a planetary magnetopause. However, for the present we will concentrate on the smooth-loading problem, leaving the treatment of these important fluctuation phenomena for a future paper; they are likely to be of diminishing importance for increasing interclump spacing to clump size ratios.

The dynamical equations are mass conservation

$$\frac{1}{r^2}\frac{\mathrm{d}r^2\rho v_r}{\mathrm{d}r} = \dot{q}, \tag{1}$$

where $\dot{q}$ is the mass-loading rate. Following Weber & Davis (1967), we assume that $v_\theta = B_\theta = 0$ so the remaining equations of motion are

$$\frac{\rho v_r}{r}\frac{\mathrm{d}r v_\phi}{\mathrm{d}r} = \frac{1}{\mu_0 r}\left(\frac{\mathrm{d}rB_\phi}{\mathrm{d}r}\right)B_r - \dot{q}v_\phi \tag{2}$$

$$\rho v_r\frac{\mathrm{d}v_r}{\mathrm{d}r} = -\frac{\mathrm{d}P}{\mathrm{d}r} - \frac{1}{\mu_0 r}B_\phi\frac{\mathrm{d}rB_\phi}{\mathrm{d}r} + \rho\frac{v_\phi^2}{r} - \dot{q}v_r, \tag{3}$$

and we assume an isothermal equation of state, $P = \rho c_\mathrm{s}^2$, where the sound speed c_s is assumed constant. Maxwell's equation $\nabla.\boldsymbol{B} = 0$ implies $r^2 B_r = const$. The non-trivial components of the flux-freezing condition,

$$\nabla \times (\boldsymbol{v} \times \boldsymbol{B}) = 0, \tag{4}$$

imply that

$$r(B_\phi v_r - B_r v_\phi) = -\Omega r^2 B_r, \tag{5}$$

where Ω is constant. Eq. (2) is integrable, to give

$$r^3\left(\rho v_r v_\phi - B_r B_\phi/\mu_0\right) = J, \tag{6}$$

and using Eq. (5), we find

$$v_\phi = \frac{Jv_r - \Omega(r^2 B_r)^2/\mu_0}{r^3\left(\rho v_r^2 - B_r^2/\mu_0\right)} \tag{7}$$

and

$$B_\phi = \frac{B_r}{r^3}\frac{J - \Omega r^4\rho v_r}{(\rho v_r^2 - B_r^2/\mu_0)}. \tag{8}$$

These equations are singular where $\rho v_r^2 = B_r^2/\mu_0$, the (radial) Alfvén condition; for the flow to pass smoothly through the radial Alfvén velocity, the numerators of the above relations must both be zero (i.e. $J/\Omega = r^4\rho v_r$). We define the radius of this critical point to be r_A, and the radial velocity at the critical point to be $v_\mathrm{A}^\star$.

The remaining r momentum equation (3), is not integrable, but can be rewritten in terms of $\mathrm{d}v_r/\mathrm{d}r$ as the singular differential equation

$$\begin{aligned}\frac{\mathrm{d}v_r}{\mathrm{d}r} = &\left\{\left[(v_\phi^2 + 2c_s^2)\frac{v_r}{r} - (v_r^2 + c_s^2)\frac{\dot{q}}{\rho}\right]\left(\rho v_r^2 - \frac{B_r^2}{\mu_0}\right)\right.\\ &\left.+\frac{B_r B_\phi}{\mu_0}v_r v_\phi\left(\frac{2v_r}{r} + \frac{\dot{q}}{\rho}\right)\right\}\\ &\Bigg/\left[\left(\rho v_r^2 - \frac{B_r^2}{\mu_0}\right)(v_r^2 - c_s^2) - \frac{B_\phi^2}{\mu_0}v_r^2\right]\end{aligned} \tag{9}$$

As in Williams et al. (1995) we assume that a wind makes a smooth transition through an X-type critical point at the outer edge of the mass-loading region. We study Parker-wind type solutions for which the flow becomes faster than the fast-mode speed as it passes outwards through that critical point, so no information from beyond the mass-loading region can propagate back into it and disrupt the steady nature of the flow there. We focus on cases in which the shock in the mass-loaded region is a fast-mode shock, because the non-evolutionary nature of intermediate-mode shocks (e.g. Falle & Komissarov 1997) implies that solutions which include them are unstable to non-axisymmetric modes.

Without loss of generality, we take $r = 1$ to be the edge of the mass-loading region, and the isothermal sound speed $c_\mathrm{s} = 1$. We assume that the integrated rate at which mass is injected into the flow distributed within this sphere is ten times the mass flux through $r = 0$. We specify the solutions of interest by the radius of the radial Alfvén critical point, r_A, the radial velocity at that point, $v_\mathrm{A}^\star$, and Ω.

3. Results

Fig. 1a shows v_r as a function of radius for various solutions with $r_\mathrm{A} = 0.5$, $v_\mathrm{A}^\star = 1.2$ and $\Omega = 1$. A constant value of $\dot{q} = 30$ was assumed for $r < 1$, with the total mass loading exceeding by a factor of ten the mass input rate at $r = 0$. Beyond $r = 1$ the mass-loading rate was $\dot{q} = 0$. The value of $\dot{q}$ sets the scaling of the density and hence the flow energy transport rate, but has no effect on the flow velocities in our formulation.

The locations of three critical points can be seen. One is at at the edge of the mass-loading region, $r = 1$. A spiral slow mode critical point is seen near $r \simeq 0.4$. Finally, there is the radial Alfvén critical point, at $r = r_\mathrm{A}$. As the parameters vary, the spiral critical point can move through the Alfvén critical point into the fast-mode regime (see Fig. 1c); for some parameters, an extra pair of slow-mode solutions appear (e.g. for the case of Fig. 1d, at the crossing of the dotted and dot-dash lines in and at the edge of the mass-loading region).

As for the sonic points in non-magnetized flows, the type of a sonic point depends on whether the curve on which the numerator is zero passes upwards through the critical (fast or slow) velocity (in which case the sonic point is X-type), or downwards (in which case the sonic point is spiral in most cases). The types of sonic points alternate with radius along the fast-mode or slow-mode critical line, but there is no constraint on the relative placement between the types of fast-mode and a slow-mode critical points. Fig. 2 shows a more detailed view of a case with the most complex form of critical points. For more on the nature of the Alfvén and slow-mode critical points, we refer the reader to the work of Zank et al. (1992) on planar mass-loaded magnetized flows.

A curve representing the loci of points corresponding to flow parameters that satisfy shock jump conditions requiring that the postshock flow pass through the fast-mode critical point at the edge of the mass-loading region is shown in Fig. 1, where the solution through the outer critical point is super-Alfvénic.

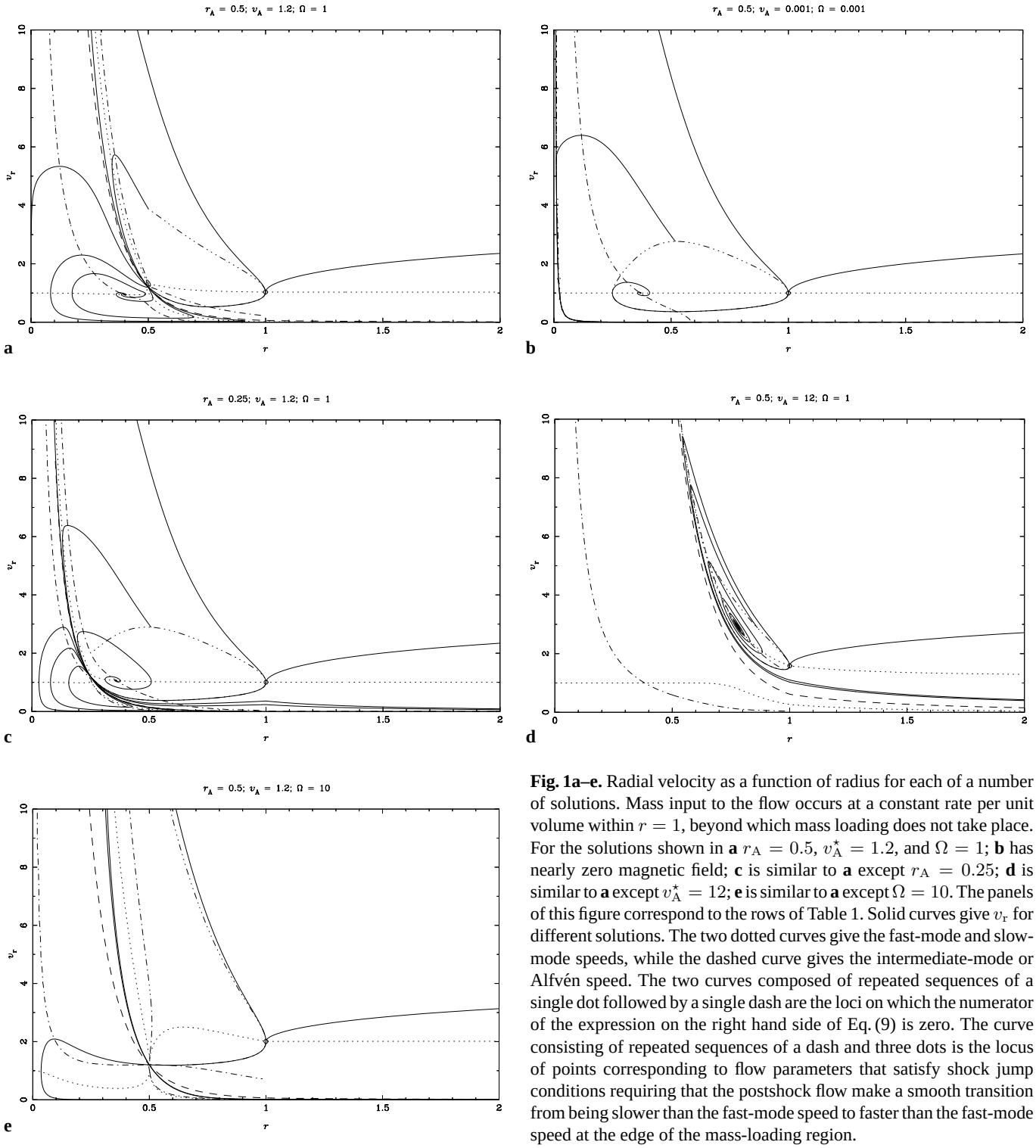

Fig. 1a–e. Radial velocity as a function of radius for each of a number of solutions. Mass input to the flow occurs at a constant rate per unit volume within $r = 1$, beyond which mass loading does not take place. For the solutions shown in **a** $r_{\rm A} = 0.5$, $v_{\rm A}^\star = 1.2$, and $\Omega = 1$; **b** has nearly zero magnetic field; **c** is similar to **a** except $r_{\rm A} = 0.25$; **d** is similar to **a** except $v_{\rm A}^\star = 12$; **e** is similar to **a** except $\Omega = 10$. The panels of this figure correspond to the rows of Table 1. Solid curves give $v_{\rm r}$ for different solutions. The two dotted curves give the fast-mode and slow-mode speeds, while the dashed curve gives the intermediate-mode or Alfvén speed. The two curves composed of repeated sequences of a single dot followed by a single dash are the loci on which the numerator of the expression on the right hand side of Eq. (9) is zero. The curve consisting of repeated sequences of a dash and three dots is the locus of points corresponding to flow parameters that satisfy shock jump conditions requiring that the postshock flow make a smooth transition from being slower than the fast-mode speed to faster than the fast-mode speed at the edge of the mass-loading region.

If this solution passes through the Alfvén critical point, an intermediate-mode shock would be required to take a fast-mode onto this solution branch; hence, for the reasons described in the previous section, we do not consider shocks onto this solution for $r < r_{\rm A}$.

Table 1 gives characteristics of some steady flow solutions. For several combinations of $r_{\rm A}$, $v_{\rm A}^\star$ and Ω we list the properties of two solutions (note that for $\Omega = 0$ the solutions pass smoothly through the radial Alfvén velocity away from the Alfvén point, while for infinitesimal Ω the solution would be singular along this line, and hence the topology of the solutions would be changed qualitatively by this infinitesimal variation in parameters). One is the solution for which the fast-mode shock is the strongest, and the other is that in which the flow just de-

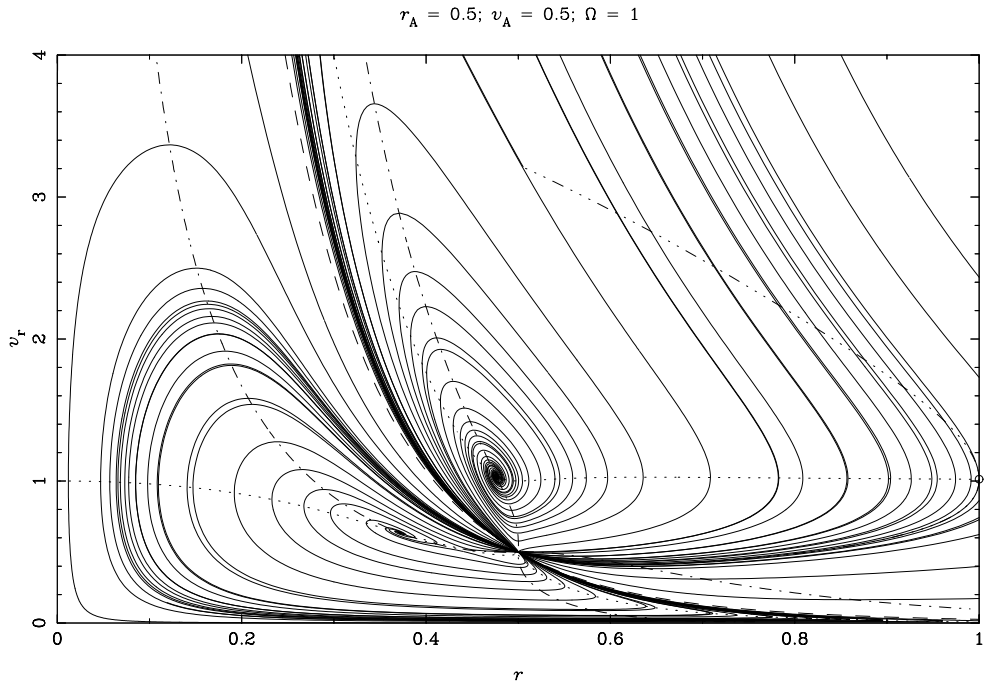

Fig. 2. Magnified view of the most complex solution topology.

Table 1. Shock and flow properties.

r_A	$v_A^\star$	Ω	M_f		L_w		M_f	L_w	
			max	shock	max	shock	max	max	$r=1$
0.5	1.2	1	3.22	3.13	22.9	22.8→13.2	6.63	87	34.0
0.5	0.001	0.001	6.40	2.77	23.3	15.1→6.13	18.8	179	33
0.25	1.2	1	4.82	2.83	21.7	15.5→6.33	13.4	149	33.1
0.5	12	1	1.34	1.31	58.9	53.9→48.9	1.45	64.7	49.6
0.5	1.2	10	9.39	6.33	233	216→66.3	9.15	276	82.8

clines to the fast-mode speed at the edge of the mass-loading region and does not include a shock. For the first solution we give the maximum fast-mode Mach number (M_f) in the flow and the fast-mode Mach number at the shock, and the values of the rate of energy transport rate (L_w) at the point where the fast-mode Mach number is the highest and on either side of the shock. The rate of energy transport per steradian is given by (cf. Weber & Davis 1967)

$$L_w = r^2 \left(\rho v_r \left[\frac{1}{2} \left(v_r^2 + v_\phi^2 \right) + \frac{\gamma}{\gamma - 1} c_s^2 \right] - \frac{\Omega r B_\phi B_r}{\mu_0} \right), \quad (10)$$

where we take $\gamma = 5/3$. The thermal energy component just scales with the mass flux, since we assume that the sound speed is maintained constant by external processes (conduction or radiative heating and cooling): we include this term primarily for comparison, and also since it is the term through which energy is added to the outward flow. For the second solution, we give the peak fast-mode Mach number as well as L_w at that peak, and at the edge of the mass-loading region.

It will be noted that several of the solutions included have maximal values of M_f on the shocked solution almost identical to those at the shock. This results from the very fast decrease of the fast-mode speed with increasing radius inside the Alfvén point. The change in radial velocity of the solution which includes the strongest shock is often weaker than this, and so while the solution is decreasing in velocity, its fast-mode Mach number is actually decreasing, and hence the maximum fast-mode Mach number is attained close to or at the radius of the shock.

In hypersonic non-magnetized mass-loaded isothermal winds, the value of the energy transport rate at the shock relative to its value where the Mach number is highest is nearly the ratio of the Mach numbers at the respective points in the flows (cf. Williams et al. 1995). This result holds because, at hypersonic velocities, the energy transport by radial velocities ($\frac{1}{2} r^2 \rho v_r^3$ in Eq. (10) above) dominates, and the momentum flux ($r^2 \rho v_r^2$ per steradian) is effectively constant. This does not hold for the energy flux as related to the fast-mode Mach number of the solutions listed here both because the fast-mode speed is a function of radius, and because the solutions are often not hyper-fast.

For the solutions presented here, the magnetic field carries only a small fraction of the energy flux, as can be seen from the panels of Fig. 3. Note in some cases, the energy flux carried by the magnetic field is inwards at small radii: apart from close to the edge of the mass-loading region, the net effect of mass loading seems to be to increase the outward transport of energy by magnetic means. The overall solution topology in each of most cases (except Fig. 1e where azimuthal component dominates) is perturbed from that of unmagnetized flows only close to the Alfvén velocity. The critical line truncates the inward limits of solutions which do not pass through the Alfvén velocity without doubling back on themselves. In this manner, a magnetic field which is unimportant for the energy fluxes still has an important effect on the global solutions.

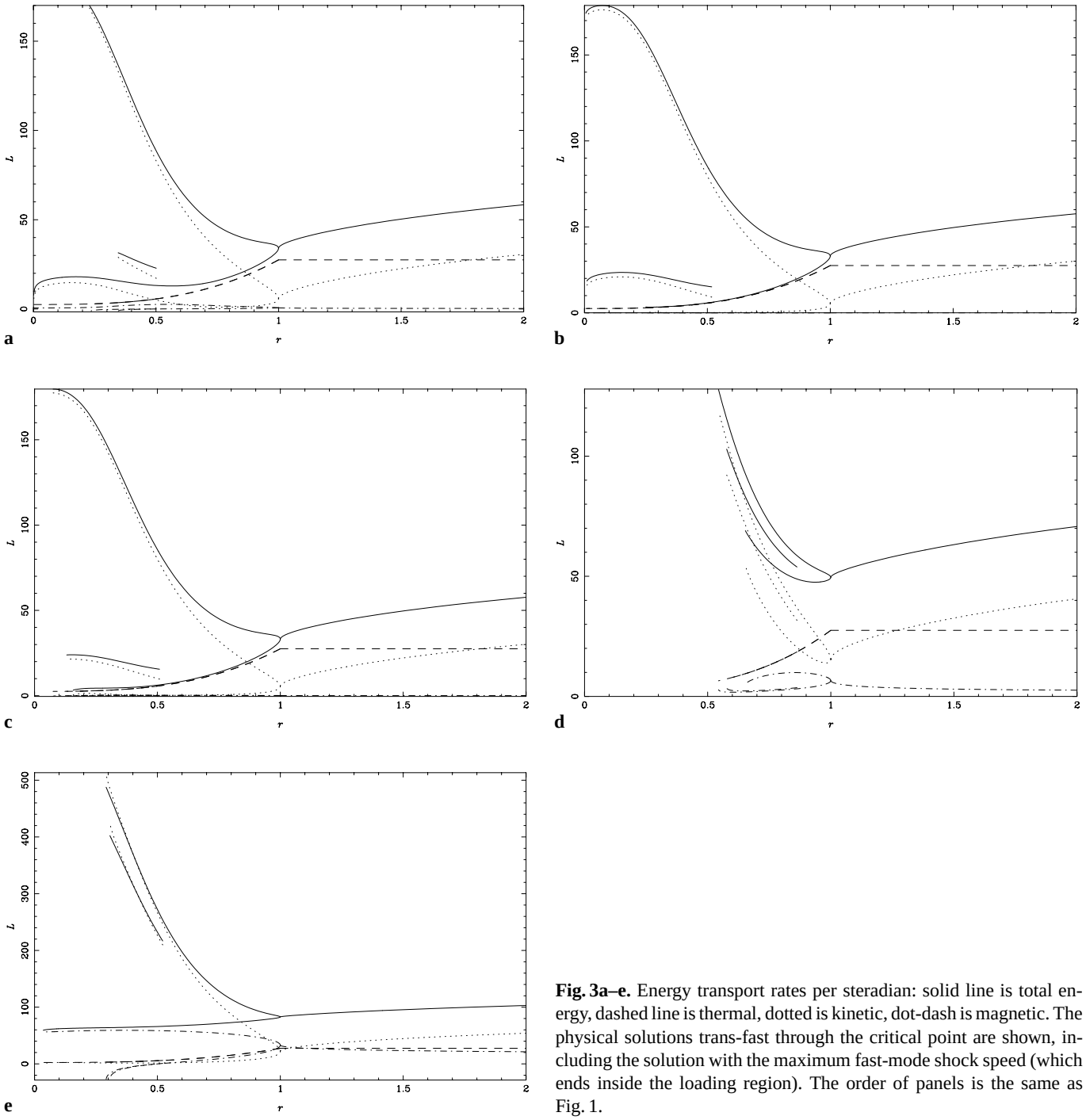

Fig. 3a–e. Energy transport rates per steradian: solid line is total energy, dashed line is thermal, dotted is kinetic, dot-dash is magnetic. The physical solutions trans-fast through the critical point are shown, including the solution with the maximum fast-mode shock speed (which ends inside the loading region). The order of panels is the same as Fig. 1.

Another effect is that, once they have reached the super-Alfvénic but sub-fast regime, solutions seem to 'coast' at a velocity close to the local radial Alfvén speed until they begin to accelerate to the edge of the mass-loading region. Examples of this are seen in Fig. 1a,c and d.

Focusing in particular on Fig. 1a, it is interesting to note that this solution has a higher velocity in the sub-Alfvénic regime than for a substantial distance beyond the mass-loading region, when it is super-fast, and that it passes through three velocity regimes as it moves outwards in radius without containing a shock. Similar velocity patterns can be obtained for unmagnetized flows, but only with rather fine-tuned values for the mass-loading law.

The values of Ω used in the present study are low when compared to characteristic stellar rotation angular velocities. For typical scaling values of distance ($10^{16}\,\mathrm{m}$) and speed ($10\,\mathrm{km\,s^{-1}}$), the solar rotation speed corresponds to $\Omega \simeq 3\times10^{6}$. However, if Ω used to parameterise the tangential magnetic field in this study were to be identified with the rotational angular velocity of the central star, the magnetic field in the

mass loading region would be tangential to one part in 3×10^7: the values, closer to unity, which we discuss give a greater feel for the true dynamics of these regions.

References

Arthur S.J., Dyson J.E., Hartquist T.W., 1994, MNRAS 269, 1117
Dgani R., Soker M., 1998, ApJ 499, L83
Dyson J.E., Hartquist T.W., Malone M.T., Taylor S.D., 1995, Rev. Mex. Astron. Astrofis. (Serie de Conferencias) 1, 119
Falle S.A.E.G., Komissarov S.S., 1997, In: Clarke D.A., West M.J. (eds.) 12th Kingston Meeting: Computational Astrophysics. Volume 123 of ASP Conf. Ser., ASP, p. 66
Malone M.T., Dyson J.E., Hartquist T.W., 1994, Ap&SS 216, 143
Raga A.C., Cantó J., Curiel S., Taylor S.D., 1998, MNRAS 295, 738
Weber E.J., Davis L. Jr., 1967, ApJ 148, 217
Williams R.J.R., Hartquist T.W., Dyson J.E., 1995, ApJ 446, 759
Zank G.P., Oughton S., Neubauer F.M., Webb G.M., 1992, JGR 97, 17051